

Supplementary Material for “Real-World Light Field Image Spatial Super-Resolution Via A Hybrid Imaging System” Part 1

Huahua Jing, Tao Yan*, Member, IEEE, Wuyang Ye, Yuan Liu, Yang Yang

In Figures 1- 3, we show our method’s aligned results on several real-world scenes. From the experimental results, it can be seen that RANSAC-Flow can well align DSLR images with the up-sampled central sub-views of the LFIs to produce considerable alignment results.

Figures 4- 15 exhibits the comparison of our method with 9 state-of-the-art super-resolution (SR) methods including classical method [1] and deep learning-based methods [2], [3], [4], [5], [6], [7], [8], [9]. It demonstrated that our proposed method obviously outperforms the other SR methods.

More experimental results can be found on our project page <https://github.com/YT3DVision/LFSR>.

REFERENCES

- [1] M. Rossi and P. Frossard, “Graph-based light field super-resolution,” in *IEEE 19th International Workshop on Multimedia Signal Processing (MMSP)*, 2017, pp. 1–6.
- [2] Y. Jo, S. W. Oh, J. Kang, and S. J. Kim, “Deep video super-resolution network using dynamic upsampling filters without explicit motion compensation,” in *Proc. IEEE CVPR*, 2018, pp. 3224–3232.
- [3] J. Jin, J. Hou, J. Chen, and S. Kwong, “Light field spatial super-resolution via deep combinatorial geometry embedding and structural consistency regularization,” in *Proc. IEEE CVPR*, 2020, pp. 2260–2269.
- [4] Y. Wang, L. Wang, J. Yang, W. An, J. Yu, and Y. Guo, “Spatial-angular interaction for light field image super-resolution,” in *Proc. ECCV*, 2020, pp. 290–308.
- [5] Z. Li, J. Yang, Z. Liu, X. Yang, and W. Wu, “Feedback network for image super-resolution,” in *Proc. IEEE CVPR*, 2019.
- [6] T. Dai, J. Cai, Y. Zhang, S.-T. Xia, and L. Zhang, “Second-order attention network for single image super-resolution,” in *Proc. IEEE CVPR*, 2019, pp. 11 065–11 074.
- [7] F. Yang, H. Yang, J. Fu, H. Lu, and B. Guo, “Learning texture transformer network for image super-resolution,” in *Proc. IEEE CVPR*, 2020, pp. 5791–5800.
- [8] N. Meng, H. K.-H. So, X. Sun, and E. Lam, “High-dimensional dense residual convolutional neural network for light field reconstruction,” *IEEE TPAMI*, 2019.
- [9] H. W. F. Yeung, J. Hou, X. Chen, J. Chen, Z. Chen, and Y. Y. Chung, “Light field spatial super-resolution using deep efficient spatial-angular separable convolution,” *IEEE TIP*, vol. 28, no. 5, pp. 2319–2330, 2018.
- [10] H. W. Fung, Yeung, Junhui, Hou, Xiaoming, Chen, Jie, Zhibo, Y. Ying, and Chung, “Light field spatial super-resolution using deep efficient spatial-angular separable convolution.” *IEEE TIP*, 2018.

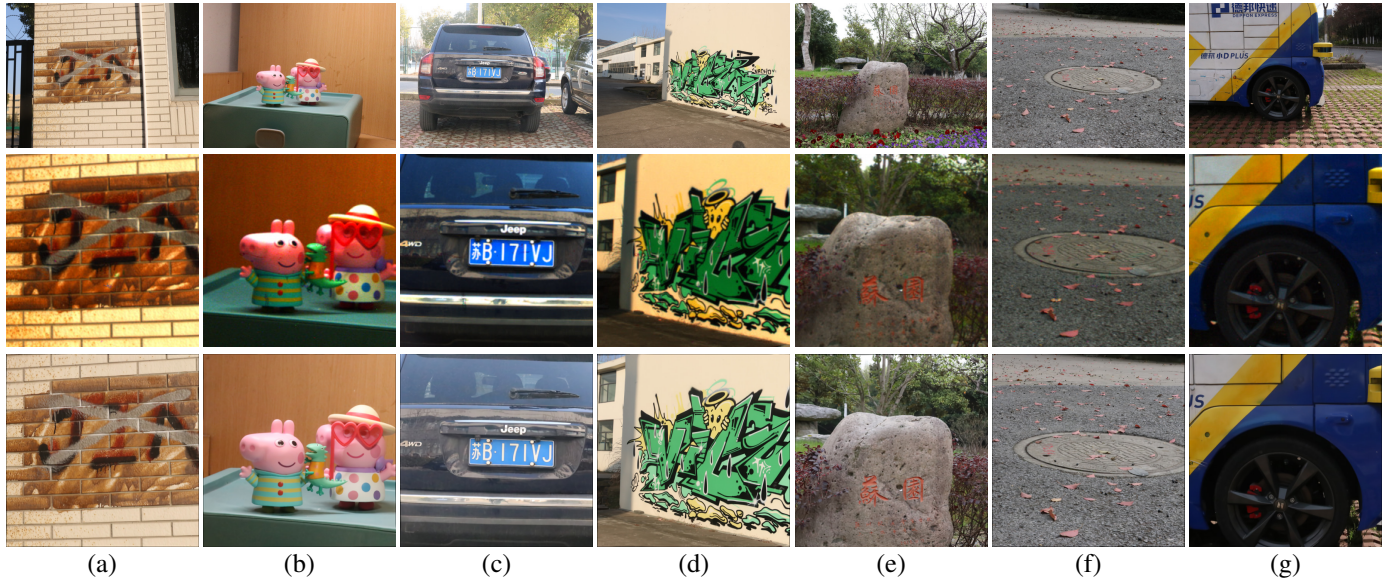


Fig. 1: From top to bottom, the first, second and third row represents the captured DSLR images, the central-views of the LFIs, and the warped DSLR images that have aligned with the upsampled central-view of the LFI.

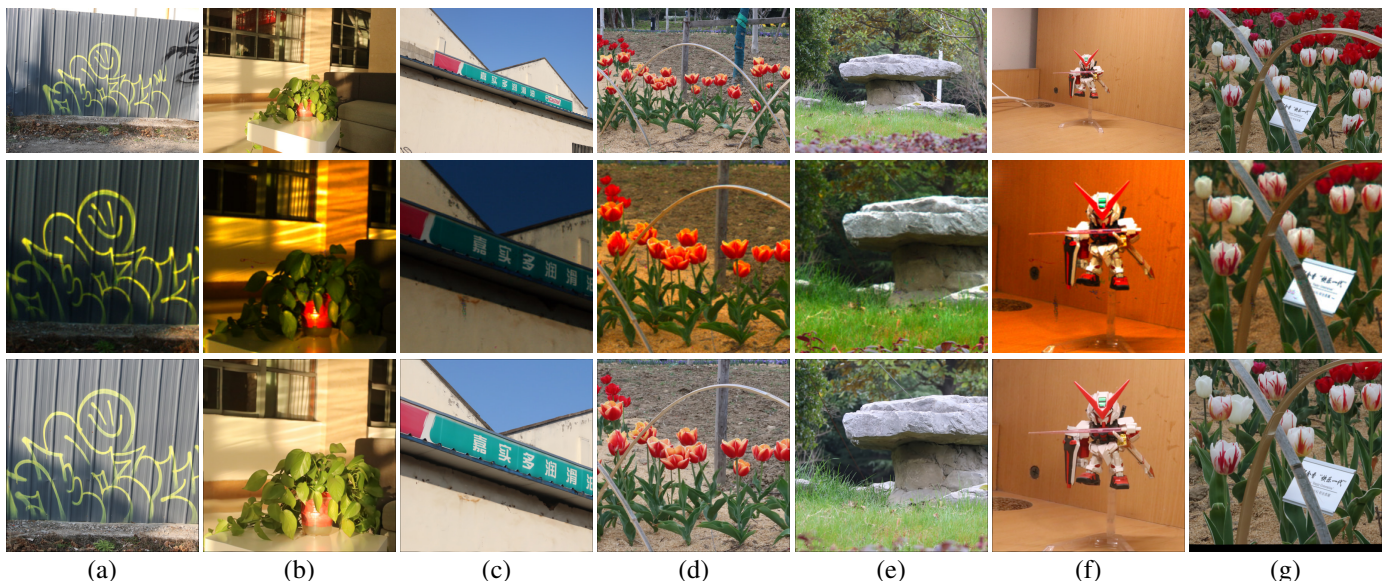


Fig. 2: From top to bottom, the first, second and third row represents the captured DSLR images, the central-views of the LFIs, and the warped DSLR images which have aligned with the upsampled central-view of the LFI.

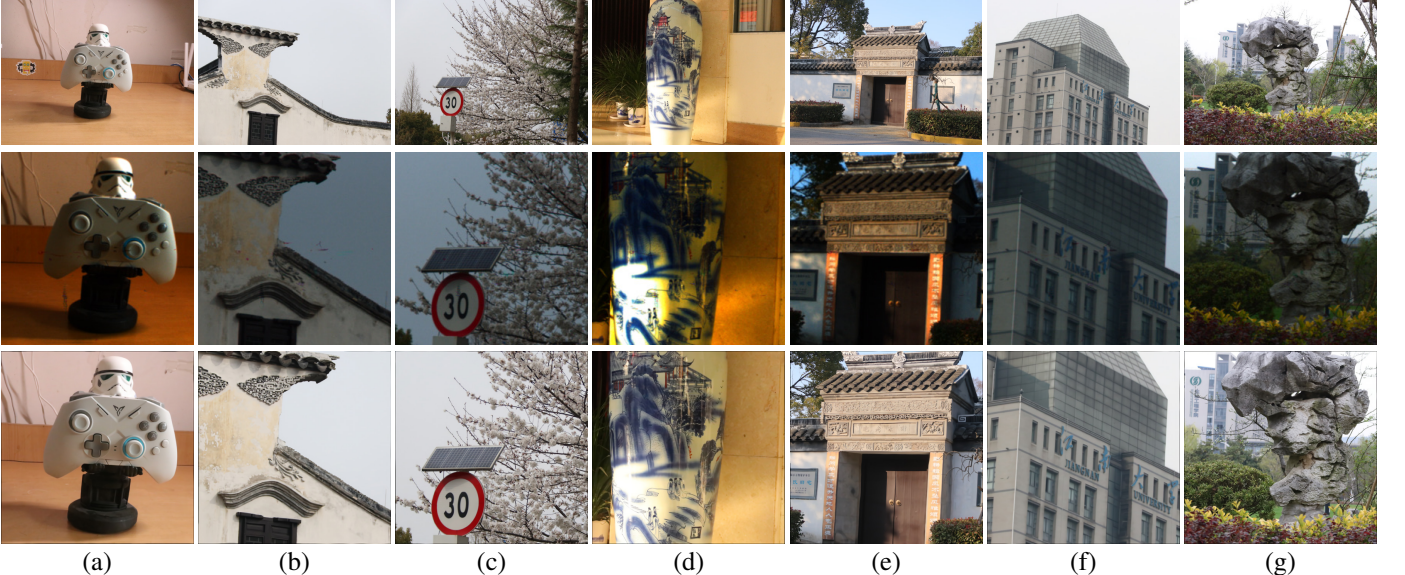


Fig. 3: From top to bottom, the first, second and third row represents the captured DSLR images, the central-views of the LFIs, and the warped DSLR images that have aligned with the upsampled central-view of the LFI.

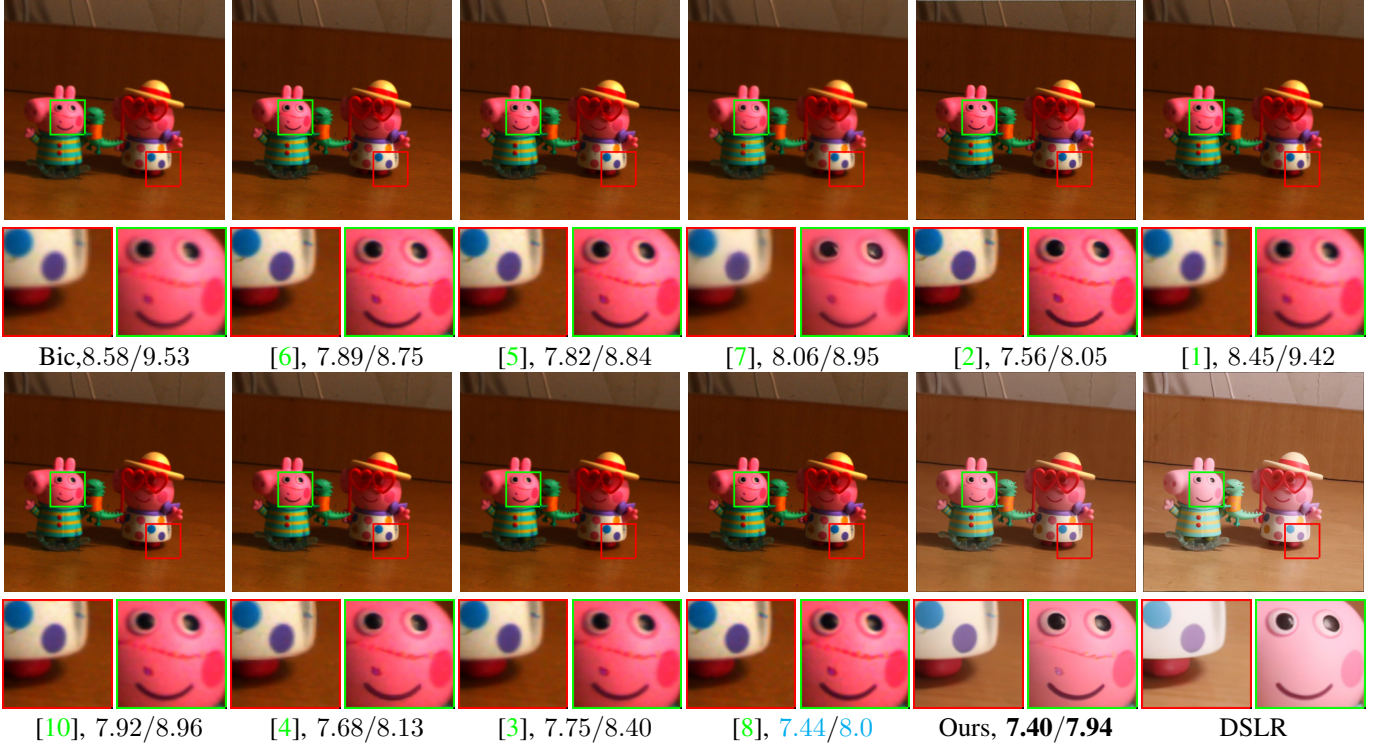


Fig. 4: Comparisons of different methods for spatially super-resolving LFIs. The super-resolution images for each method is marked with its PI/NIQE values. The best value is marked in **bold**, and the second best is marked in **cyan**.

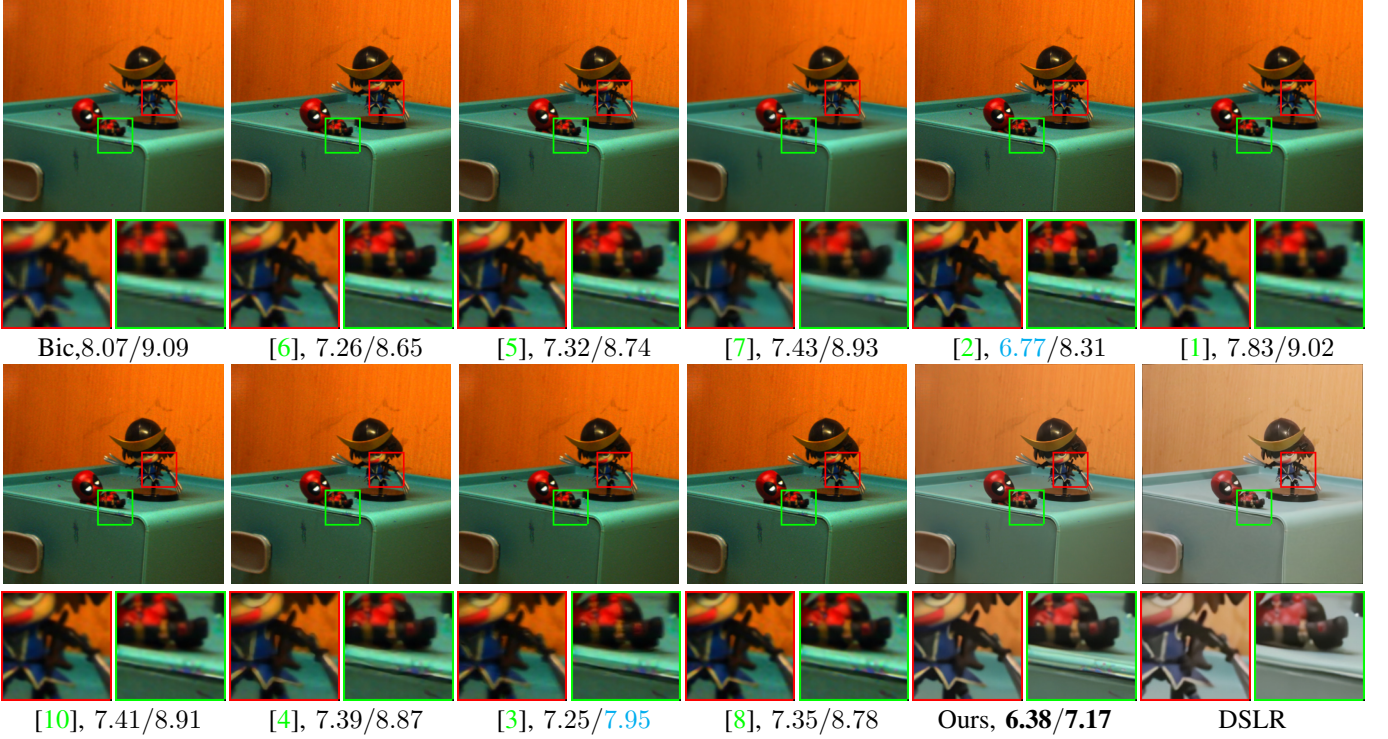


Fig. 5: Comparisons of different methods for spatially super-resolving LFIs. The super-resolution images for each method is marked with its PI/NIQE values. The best value is marked in **bold**, and the second best is marked in **cyan**.

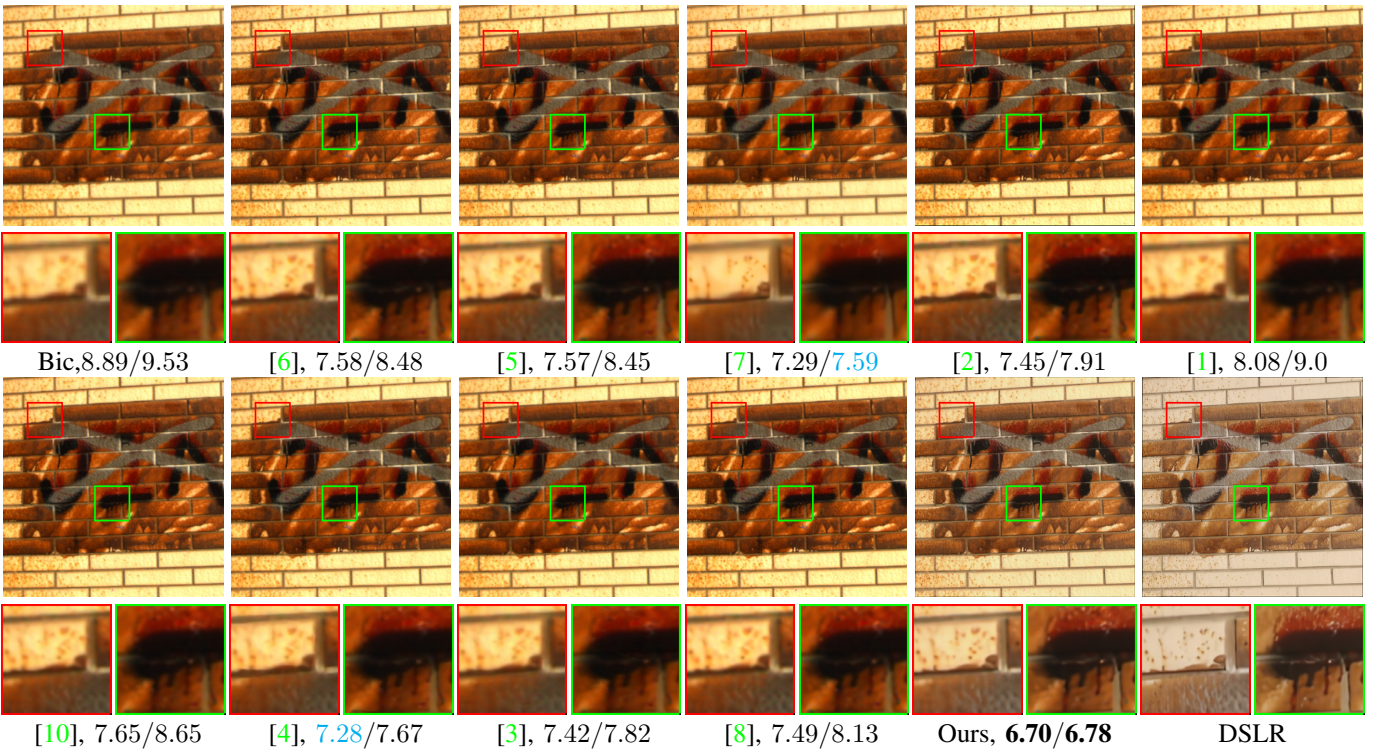


Fig. 6: Comparisons of different methods for spatially super-resolving LFIs. The super-resolution images for each method is marked with its PI/NIQE values. The best value is marked in **bold**, and the second best is marked in **cyan**.

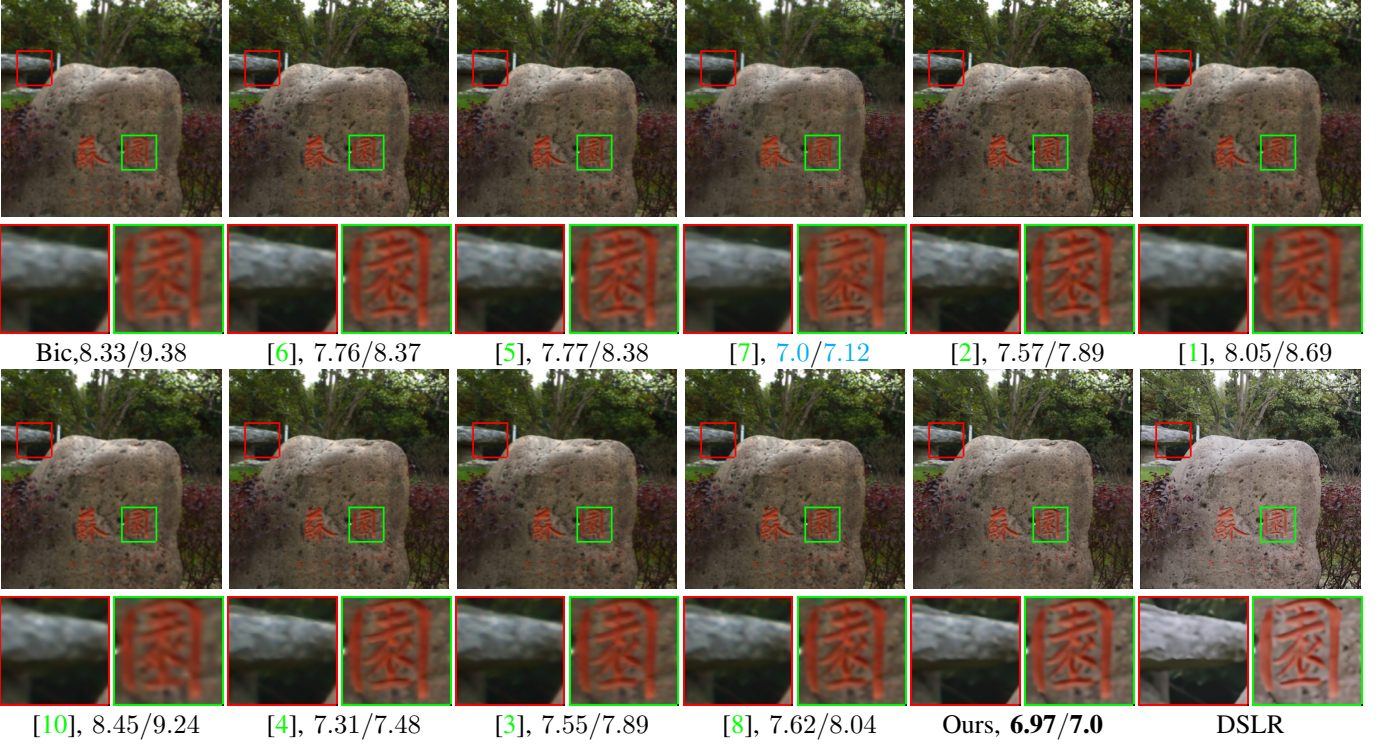


Fig. 7: Comparisons of different methods for spatially super-resolving LFIs. The super-resolution images for each method is marked with its PI/NIQE values. The best value is marked in **bold**, and the second best is marked in **cyan**.

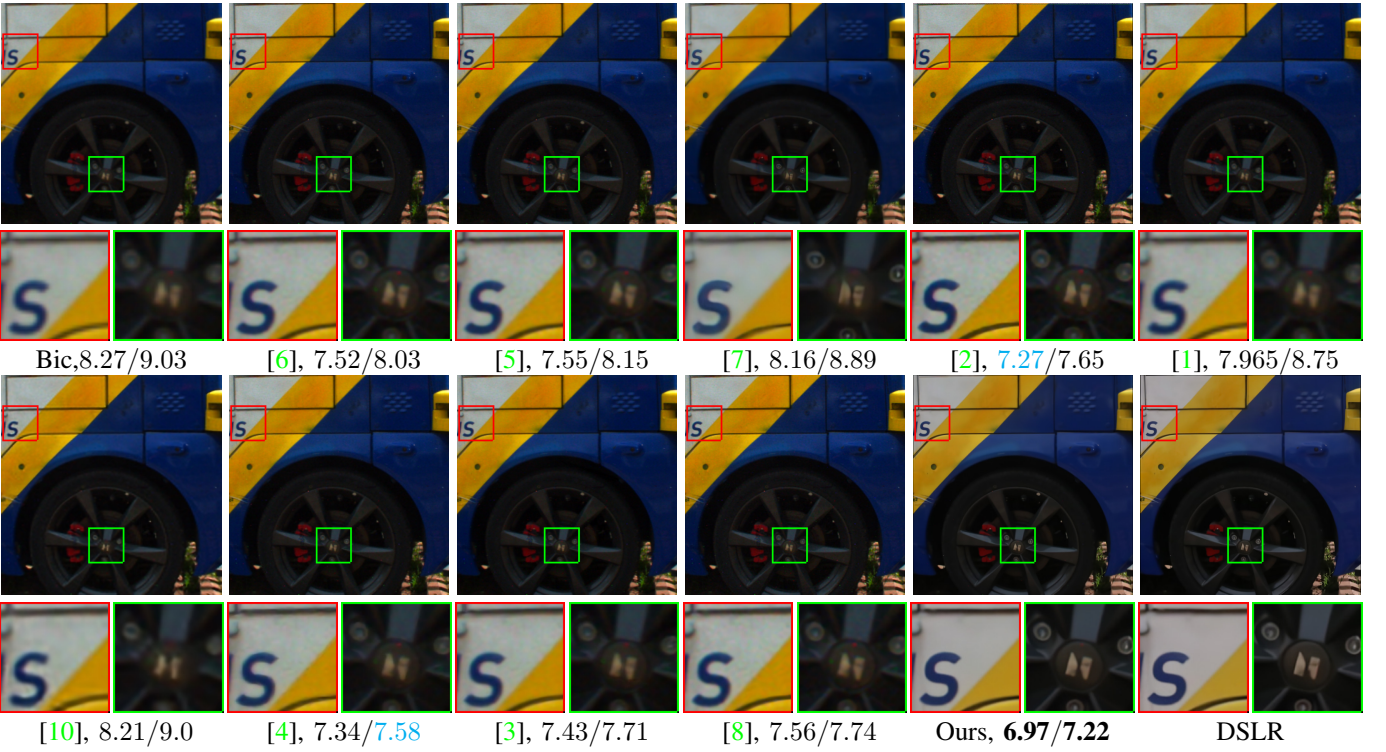


Fig. 8: Comparisons of different methods for spatially super-resolving LFIs. The super-resolution images for each method is marked with its PI/NIQE values. The best value is marked in **bold**, and the second best is marked in **cyan**.

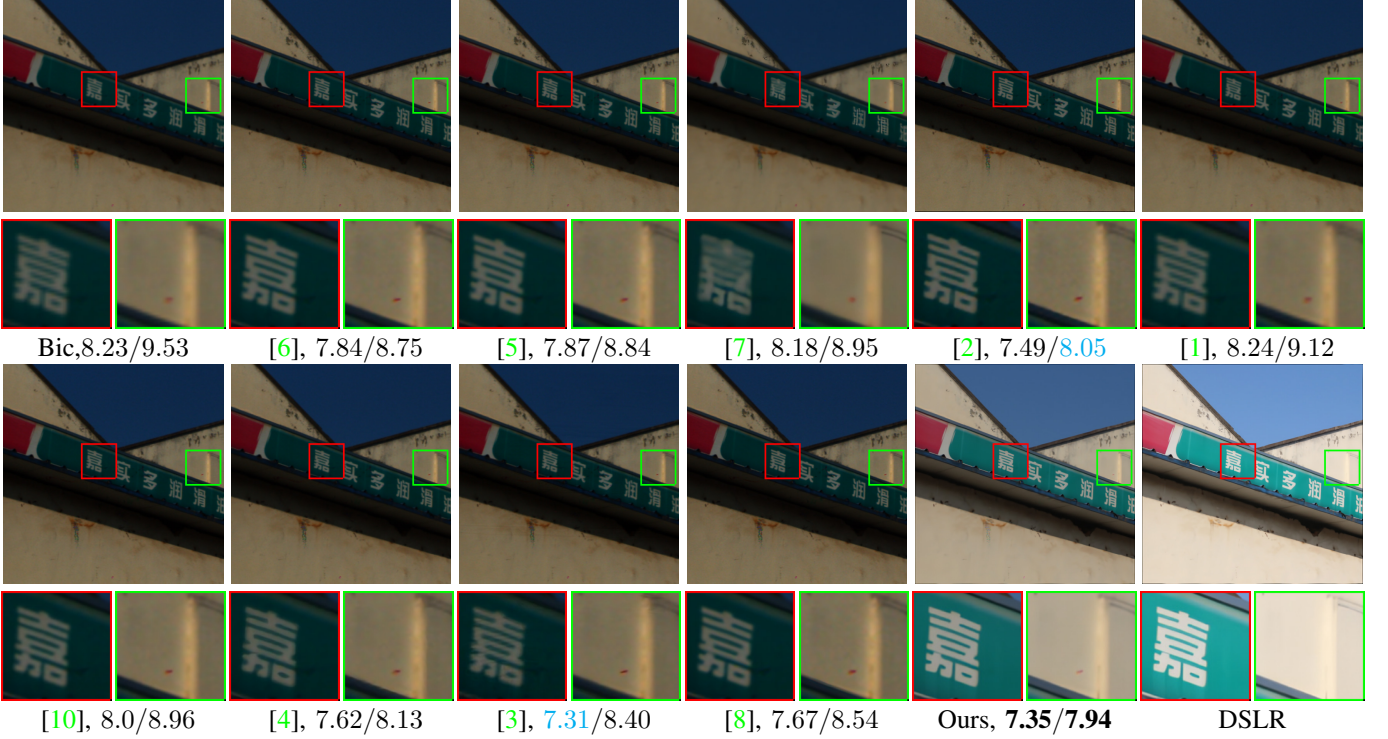


Fig. 9: Comparisons of different methods for spatially super-resolving LFIs. The super-resolution images for each method is marked with its PI/NIQE values. The best value is marked in **bold**, and the second best is marked in **cyan**.

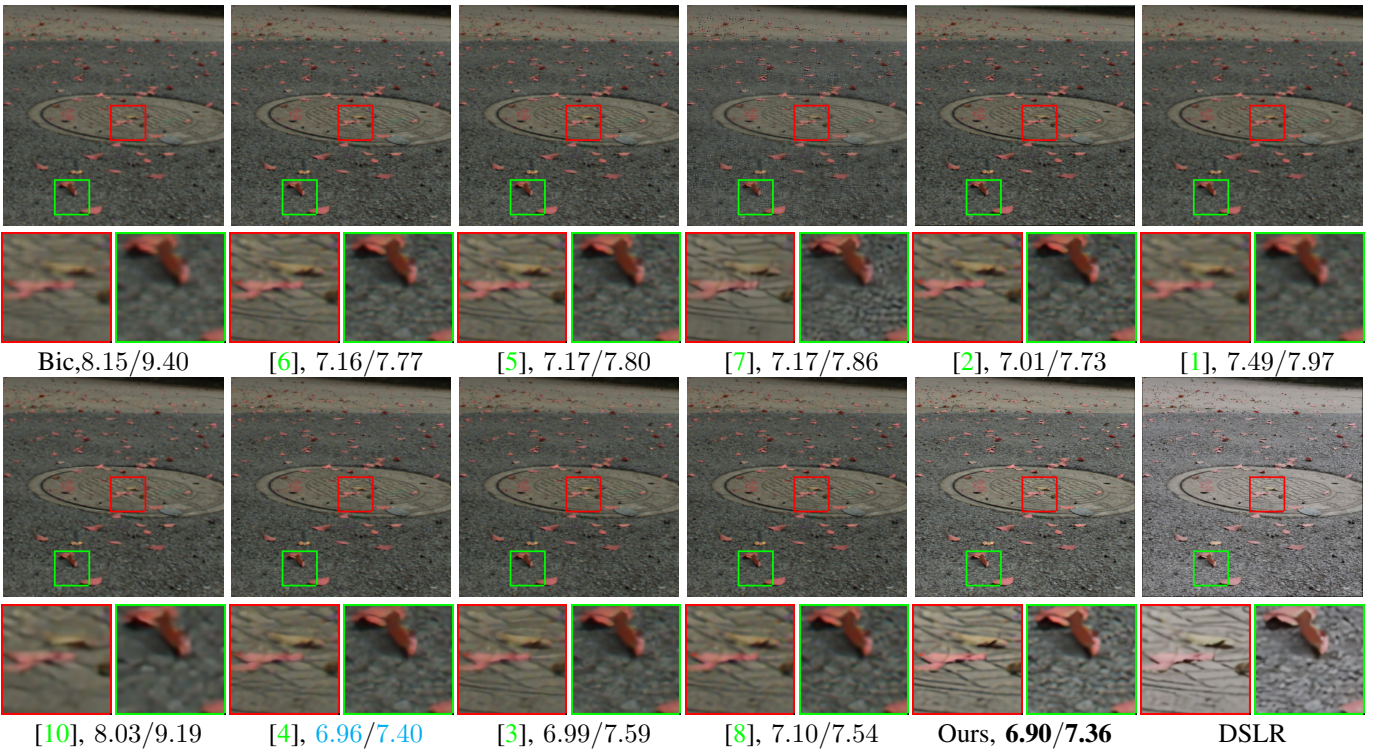


Fig. 10: Comparisons of different methods for spatially super-resolving LFIs. The super-resolution images for each method is marked with its PI/NIQE values. The best value is marked in **bold**, and the second best is marked in **cyan**.

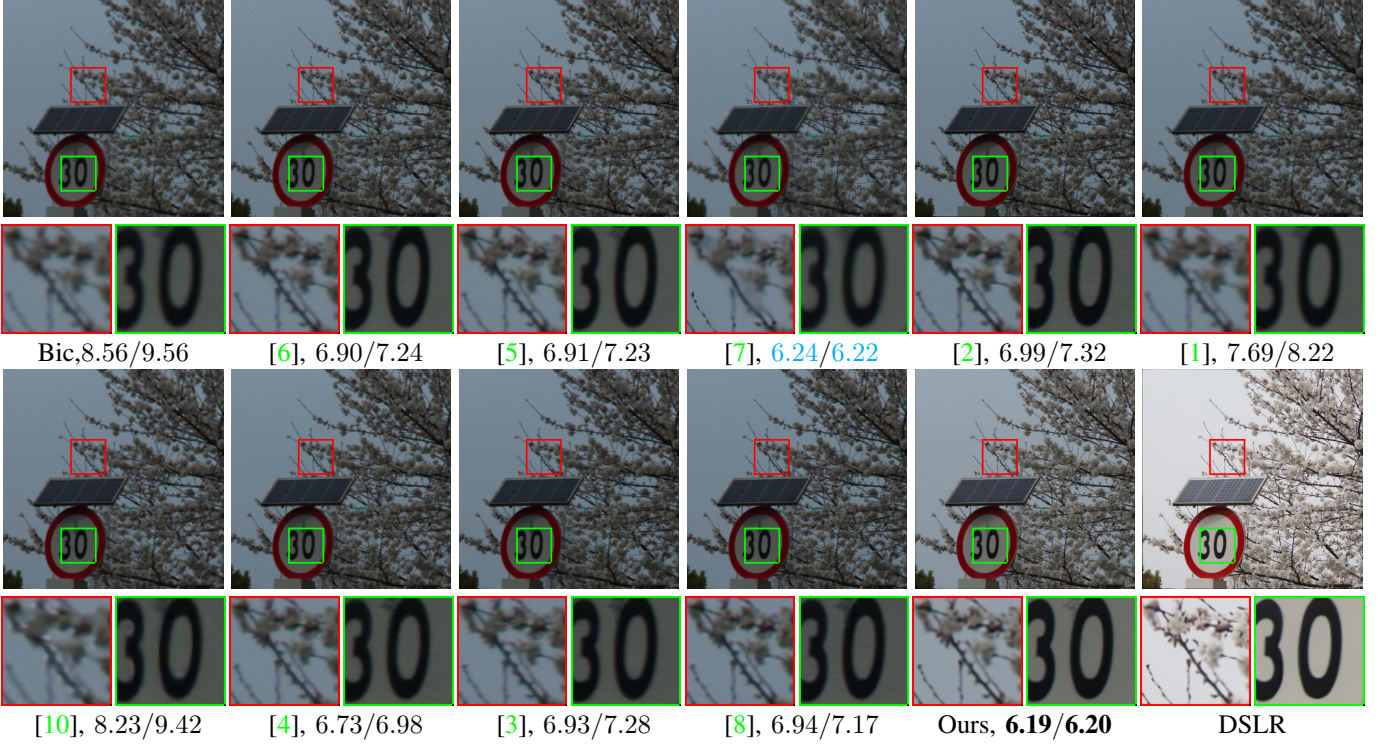


Fig. 11: Comparisons of different methods for spatially super-resolving LFIs. The super-resolution images for each method is marked with its PI/NIQE values. The best value is marked in **bold**, and the second best is marked in **cyan**.

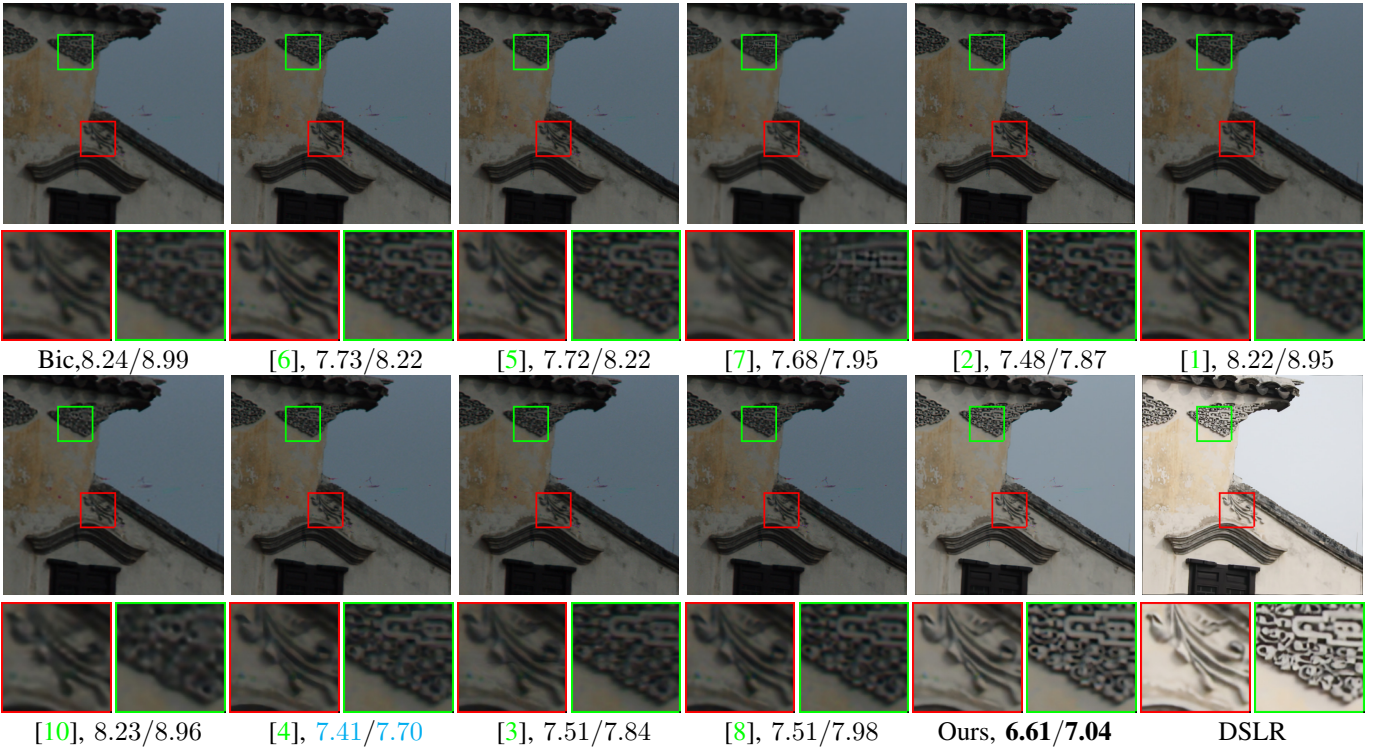


Fig. 12: Comparisons of different methods for spatially super-resolving LFIs. The super-resolution images for each method is marked with its PI/NIQE values. The best value is marked in **bold**, and the second best is marked in **cyan**.

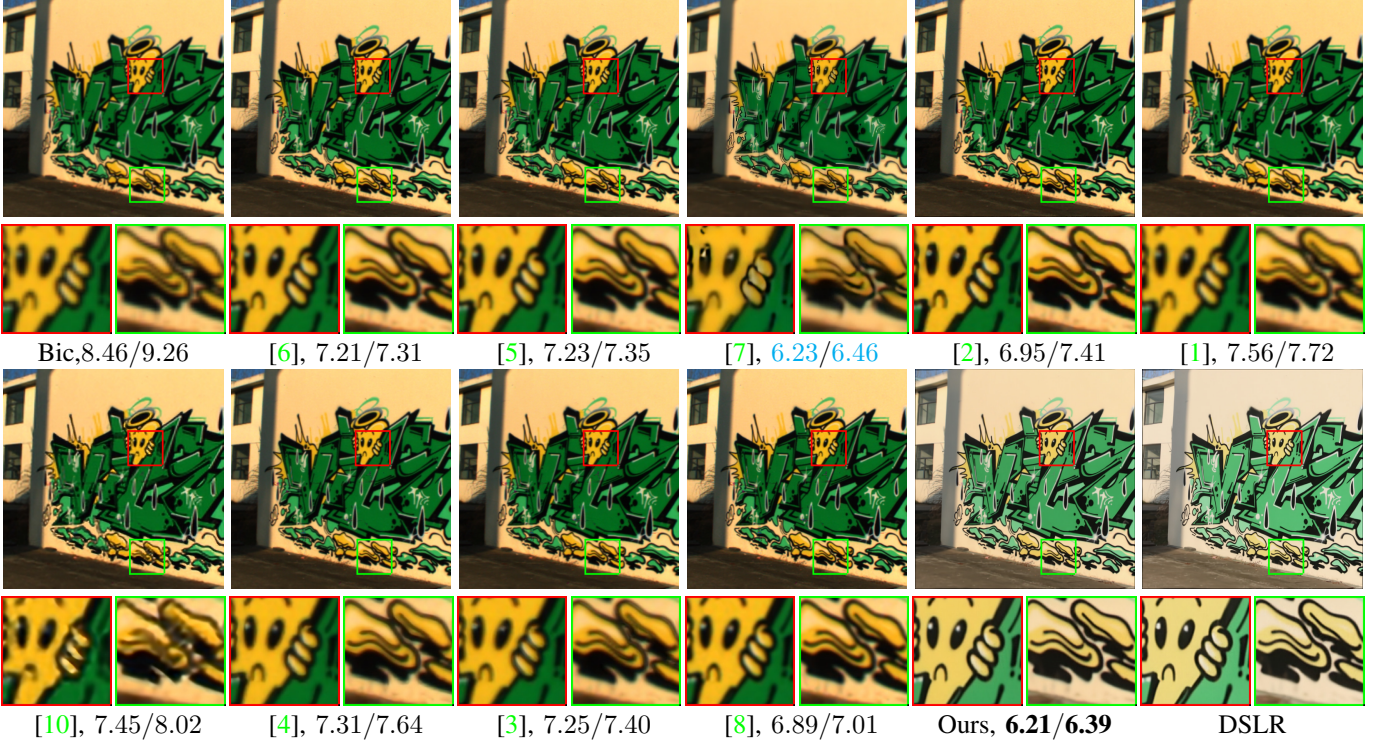


Fig. 13: Comparisons of different methods for spatially super-resolving LFIs. The super-resolution images for each method is marked with its PI/NIQE values. The best value is marked in **bold**, and the second best is marked in **cyan**.

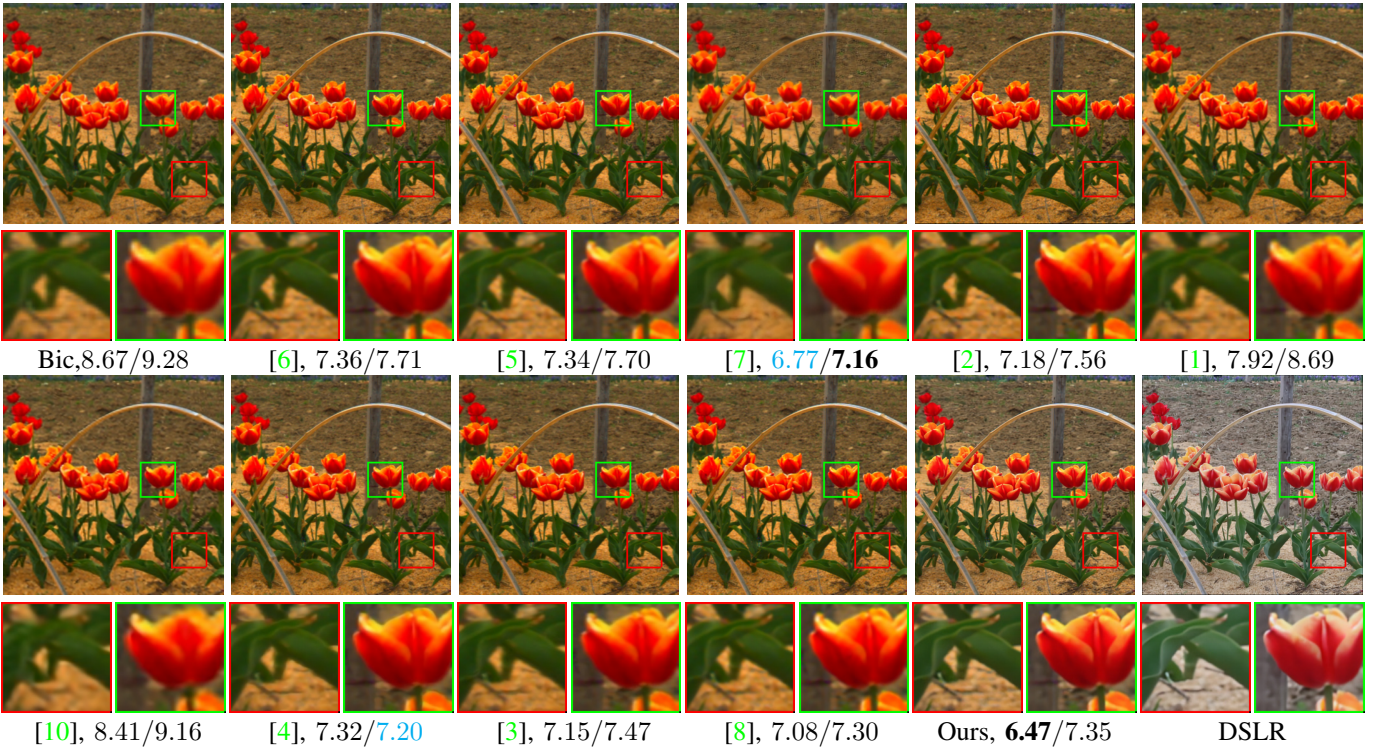


Fig. 14: Comparisons of different methods for spatially super-resolving LFIs. The super-resolution images for each method is marked with its PI/NIQE values. The best value is marked in **bold**, and the second best is marked in **cyan**.

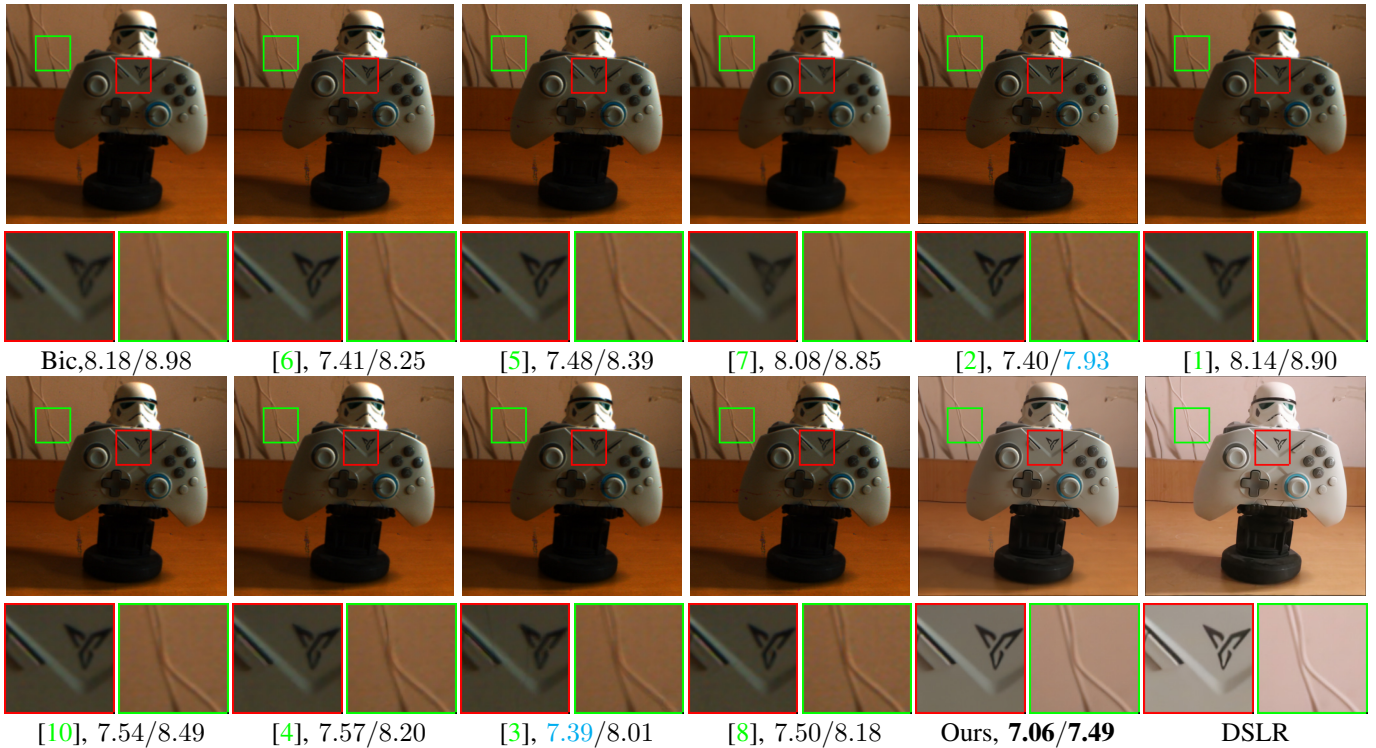


Fig. 15: Comparisons of different methods for spatially super-resolving LFIs. The super-resolution images for each method is marked with its PI/NIQE values. The best value is marked in **bold**, and the second best is marked in **cyan**.